IEEE Access
Multidisciplinary | Rapid Review | Open Access Journal

Received 31 October 2023, accepted 11 November 2023, date of publication 14 November 2023,
date of current version 21 November 2023.

Digital Object Identifier 10.1109/ACCESS.2023.3332991

RESEARCH ARTICLE

Direction-of-Arrival Estimation Based on Sparse Representation of Fourth-Order Cumulants

CHUANXI XING, SAIMENG DONG, AND ZHILIANG WAN
School of Electrical and Information Technology, Yunnan Minzu University, Kunming 650504, China
Yunnan Key Laboratory of Unmanned Autonomous System, Kunming 650504, China

Corresponding author: Saimeng Dong (dongsaimeng@163.com)

This work was supported in part by the National Natural Science Foundation of China under Grant 61761048; and in part by the Basic Research Special General Project of Yunnan Province, China, under Grant 202101AT070132.

ABSTRACT The actual underwater environmental noise is often spatial colored, which results in severe degradation of the performance of the underwater direction of arrival (DOA) estimation method based on the assumption of white noise. In the presence of Gaussian colored noise, a high-resolution DOA estimation method using a fourth-order cumulant for quickly eliminating redundancy is adopted in this paper. Firstly, a selection matrix is constructed, and the redundant data in the fourth-order cumulants are reduced in the way of descending order. Secondly, the fourth-order cumulants matrix is transformed into a vectorized form, and the selection matrix is further constructed to eliminate redundant data in the vectorization process, and a single observation vector model with better performance is obtained. Finally, the sparse representation method is used for DOA estimation. The simulation results demonstrate that compared with the traditional fourth-order cumulant methods, this method has a stronger ability to suppress colored noise, and can provide higher resolution and higher estimation accuracy under the conditions of few snapshots and low signal-to-noise ratio. The experiment verifies that this method can be applied to DOA estimation of underwater acoustic array signals.

INDEX TERMS Colored noise, underwater acoustic targets, direction of arrival estimation, fourth-order cumulant, sparse representation.

I. INTRODUCTION

In ocean acoustic research, underwater direction of arrival (DOA) estimation has been a hot topic for scholars [1], [2], [3], [4]. In the current study, most of the algorithms are effective only in the white noise environment of the array element noise, however, the actual underwater environment is affected by the noise of distant ships, wind noise, biological sounding, etc., the background noise is often colored, and the performance of the DOA estimation methods applicable to white noise will be seriously degraded [5], [6], [7], [8], [9].

In recent years, the theory of compressive sensing (CS) has been developed, and sparse signal reconstruction (SSR) techniques are gradually used in the field of array signal processing [10], [11], [12]. Many scholars proposed the L1-paradigm class method [13], [14], which realizes the DOA estimation by discretizing the null domain and solving it using the L1-paradigm constrained model, and the advantage of this class method is that the computational complexity does not increase with the increase of the number of snapshots, and it has a high resolution of the measurement direction. Yang et al. proposed the off-grid sparse Bayesian inference (OGSBI) algorithm [15], which not only ensures that the proposed solution is the global optimal solution, but also has a high computational efficiency and realizes high-accuracy off-grid DOA estimation under coarse grid conditions.

The above algorithms are all based on the assumption of Gaussian white noise, and scholars at home and abroad have proposed many methods for the problem of DOA estimation in the context of colored noise. In 1995, the scholar B. Porat combined the fourth-order cumulant and rotationally invariant subspace estimation of signal parameter via

The associate editor coordinating the review of this manuscript and approving it for publication was Xuebo Zhang.

rotational invariance techniques (ESPRIT) direction finding algorithm [16], replacing the traditional covariance matrix with the fourth-order cumulant matrix, and suppressing the colored noise by using the fourth-order cumulant. After that, S. J. Wu et al. proposed a reduced-order MUSIC-like array extension method [17], which extends the array aperture, but the computation is still large. H. Y. Song et al. from Harbin Engineering University proposed a high-resolution method based on orthogonal joint diagonalization of groups of higher-order cumulant matrices for hydroacoustic target orientation estimation [18], which is also applicable under coherent source conditions, but requires the construction of multiple higher-order cumulant matrices, which is computationally intensive. S. N. Han et al. proposed a fourth-order cumulant sparse representation method by singular value decomposition of the fourth-order cumulant matrix of the array received data and solving it by using the paradigm theory, which has a limited estimation accuracy when the signal-to-noise ratio is low [19]. Liu et al. proposed a sparse representation of non-redundant cumulants [20], which effectively suppresses the correlated colored noise and reduces the complexity of the sparse solution. Literature [21] utilizes a parametric approach to jointly estimate the DOA and noise parameters, but the structural properties of the noise covariance matrix need to be known. Literature [22] combines the covariance matrix difference method with an off-grid DOA method to obtain a high estimation accuracy, but at the expense of the array aperture, mirror artifacts occur.

In this paper, we propose a novel method that combines fourth-order cumulation and sparse representation to improve DOA estimation accuracy in the presence of Gaussian colored noise. The fourth-order accumulation and sparse representation are combined to filter out Gaussian colored noise and extend the array aperture by calculating the fourth-order accumulation of the array received signal, which reduces the computational complexity and further extends the array aperture by removing the redundant data twice, improves the resolution of the target and obtains a higher array gain. The orientation estimation accuracy is improved with the help of the sparsity of the signal in the airspace. The method is applied to hydroacoustic target orientation estimation and effectively suppresses colored noise, extends the array aperture, and improves target resolution and accuracy in hydroacoustic target orientation estimation.

The paper is structured as follows: Section I outlines the challenges posed by colored noise in real underwater environments and describes several algorithms proposed to address this problem internationally. Section II introduces the signal reception model used in this study. Section III describes our proposed DOA algorithm centered on sparse representation and elaborates on the theory behind fourth-order accumulation and sparse representation. Section IV simulates and analyzes a comparison between the similar MUSIC-like algorithm, the OGSBI algorithm, and the algorithm proposed in this paper. The section also details the sources of the experimental data collected during the sea trials, which were used to validate the performance of the algorithms. The conclusions are given in Section V.

II. DOA ESTIMATION MODE

A M-element uniform hydrophone array with array element spacing d is used for hydroacoustic signal localization. Under the plane wave assumption [23], the signals from K far-field sources are incident on the hydrophone array in wave direction θ, $\boldsymbol{\theta}=[\theta_1, \theta_2, \cdots, \theta_K]^T$. The model schematic is shown in Figure. 1, and at the moment t, the observation model received by the array can be expressed as

$$\boldsymbol{y}(t) = \boldsymbol{A}(\theta)\boldsymbol{x}(t) + \boldsymbol{e}(t),\ t = 1, 2, \cdots, T, \tag{1}$$

where $\boldsymbol{y}(t) = [y_1(t), y_2(t), \cdots, y_M(t)]^T$ is the array received signal, $\boldsymbol{x}(t)=[x_1(t), x_2(t), \cdots, x_K(t)]^T$ is the source signal vector, $\boldsymbol{e}(t) = [e_1(t), e_2(t), \cdots, e_M(t)]^T$ is the noise vector, T denotes the number of snapshots, $\boldsymbol{\theta}$ denotes the set of incidence directions of the K signals, and $\boldsymbol{A}(\theta) = [\boldsymbol{a}(\theta_1), \boldsymbol{a}(\theta_2), \cdots, \boldsymbol{a}(\theta_K)]$ is the array flow matrix. Where $\boldsymbol{a}(\theta_k) = [1, \nu_{\theta_k}, \cdots, \nu_{\theta_k}^{M-1}]$, $\nu_{\theta_k} = e^{-j2\pi d/\lambda \sin(\theta_k)}$, λ is the wavelength of the signals, $\boldsymbol{a}_m(\theta_k)$ contains the delay information of the kth signal received by the first array sensor.

Then the DOA estimation model in the case of multiple observation vectors can be expressed as

$$\boldsymbol{Y} = \boldsymbol{A}(\theta)\boldsymbol{X} + \boldsymbol{E}, \tag{2}$$

where $\boldsymbol{Y} = [\boldsymbol{y}(1), \boldsymbol{y}(2), \cdots, \boldsymbol{y}(T)]$ is the received signal matrix, $\boldsymbol{X} = [\boldsymbol{x}(1), \boldsymbol{x}(2), \cdots, \boldsymbol{x}(T)]$ is the source signal amplitude matrix, and $\boldsymbol{E} = [\boldsymbol{e}(1), \boldsymbol{e}(2), \cdots, \boldsymbol{e}(T)]$ is the noise matrix.

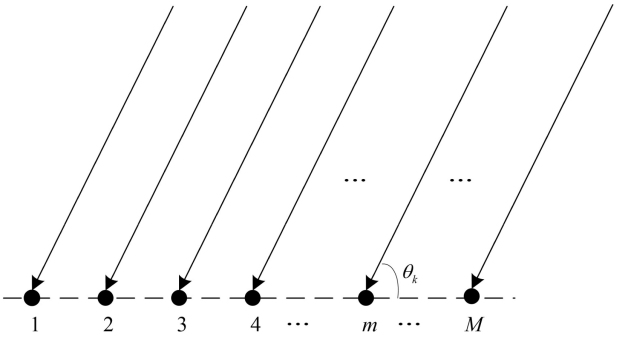

FIGURE 1. Schematic diagram of signal arrival at array element.

III. DOA ALGORITHM FOR SPARSE REPRESENTATION

The algorithm of the paper is based on the problem of DOA estimation in the context of Gaussian colored noise. Initially, sparse representation is considered, and the fourth-order cumulants of the observed signals are transformed to eliminate redundancy and reduce dimensionality through the creation of a selection matrix. Secondly, the fourth-order cumulant matrix is transformed into a vectorized form,

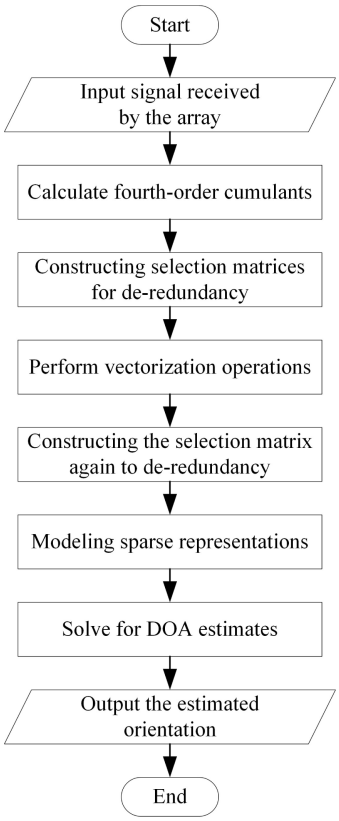

FIGURE 2. Flowchart of the DOA algorithm using fourth-order cumulant to eliminate redundancy.

and a selection matrix is assembled to eliminate redundant data in the vectorization process, resulting in a superior, single-observation vector model. finally, the algorithm creates a sparse representation model, which solves the L-1 paradigm sparse constraint optimization problem, enabling the calculation of DOA estimations. The overall flow of the algorithm is shown in Figure. 2.

A. FOURTH-ORDER CUMULATIVE QUANTITY

Theoretically fourth-order cumulants can completely suppress Gaussian colored noise and to some extent other colored noise as well [24], [25]. When the incident signal source is non-Gaussian and the noise is Gaussian colored noise, the fourth-order cumulant matrix of the received data from the shallow-sea acoustic field array is

$$\begin{aligned}\boldsymbol{C}_{4y}(i,j,n,l) &= \mathrm{cum}(y_i, y_j, y_n^*, y_l^*) \\ &= \mathrm{E}[y_i y_j y_n^* y_l^*] - \mathrm{E}[y_i y_n^*]\mathrm{E}[y_j y_l^*] \\ &\quad - \mathrm{E}[y_i y_l^*]\mathrm{E}[y_j y_n^*] - \mathrm{E}[y_i, y_j]\mathrm{E}[y_n^* y_l^*], \end{aligned} \tag{3}$$

where $(\cdot)^*$ denotes the covariance. The fourth-order cumulant $\boldsymbol{C}_{4y}$ has M^4 elements, and the range of the variables in (3) is $1 \le i, j, n, l \le M$, and these elements are put into the $M^2 \times M^2$ covariance matrix $\boldsymbol{C}$. The $\{(i-1)M + j, (n-1)M + l\}$ th element of matrix $\boldsymbol{C}$ corresponds to $\boldsymbol{C}_{4y}(i, j, n, l)$ and matrix $\boldsymbol{C}$ can be expressed as

$$\begin{aligned}\boldsymbol{C} &= \mathrm{E}\{(\boldsymbol{Y} \otimes \boldsymbol{Y}^*)(\boldsymbol{Y} \otimes \boldsymbol{Y}^*)^{\mathrm{H}}\} \\ &\quad - \mathrm{E}\{\boldsymbol{Y} \otimes \boldsymbol{Y}^*\}\mathrm{E}\{(\boldsymbol{Y} \otimes \boldsymbol{Y}^*)^{\mathrm{H}}\} \\ &\quad - \mathrm{E}\{\boldsymbol{Y}\boldsymbol{Y}^{\mathrm{H}}\} \otimes \mathrm{E}\{(\boldsymbol{Y}\boldsymbol{Y}^{\mathrm{H}})^*\}, \end{aligned} \tag{4}$$

where $\otimes$ denotes the Kronecker product. The fourth order cumulant matrix of the signal is

$$\begin{aligned}\boldsymbol{C}_x &= \mathrm{E}\{(\boldsymbol{X} \otimes \boldsymbol{X}^*)(\boldsymbol{X} \otimes \boldsymbol{X}^*)^{\mathrm{H}}\} \\ &\quad - \mathrm{E}\{\boldsymbol{X} \otimes \boldsymbol{X}^*\}\mathrm{E}\{(\boldsymbol{X} \otimes \boldsymbol{X}^*)^{\mathrm{H}}\} \\ &\quad - \mathrm{E}\{\boldsymbol{X}\boldsymbol{X}^{\mathrm{H}}\} \otimes \mathrm{E}\{(\boldsymbol{X}\boldsymbol{X}^{\mathrm{H}})^*\}, \end{aligned} \tag{5}$$

where the fourth-order cumulant $\boldsymbol{C}_x$ of the signal is a $K^2 \times K^2$ dimensional matrix, and its $\{(i-1)K + j, (n-1)K + l\}$th element can be expressed as $cum(x_i, x_j, x_n^*, x_l^*), \forall i, j, n, l \in \{1, 2, \cdots, K\}$. According to the nature of the fourth-order cumulant, the Gaussian noise term is filtered out, which can be obtained as

$$\boldsymbol{C} = (\boldsymbol{A}(\theta) \otimes \boldsymbol{A}(\theta)^*)\boldsymbol{C}_x(\boldsymbol{A}(\theta) \otimes \boldsymbol{A}(\theta)^*)^{\mathrm{H}}. \tag{6}$$

Based on the nature of the fourth-order cumulants, the following relation can be derived:

$$\boldsymbol{C}_x = \mathrm{cum}(x_i, x_j, x_n^*, x_l^*) = \begin{cases} \neq 0, & i = j = n = l \\ = 0, & \text{else.} \end{cases} \tag{7}$$

From (7), we can see that only K elements in $\boldsymbol{C}_x$ are nonzero, and these elements are located on the diagonal of $\boldsymbol{C}_x$, i.e., $(i-1)K + i (i = 1, \cdots, K)$th element of the diagonal of C is nonzero. The fourth-order cumulant matrix of the signal can be reduced to a diagonal matrix by removing all the elements of the matrix $\boldsymbol{C}_x$ that are zero-valued and downgrading the matrix $\boldsymbol{C}_x$. The order of the matrix can be reduced from $K^2 \times K^2$ to $K \times K$, which gives

$$\bar{\boldsymbol{C}}_x = \mathrm{diag}(\gamma_{x_1}, \gamma_{x_2}, \cdots, \gamma_{x_K}), \tag{8}$$

where $\gamma_{s_k} = cum(x_i, x_j, x_n^*, x_l^*) = \boldsymbol{C}_x((i-1)K + i, (i-1)K + i)$.

The fourth-order cumulative quantity of the new array received data obtained after the dimensionality reduction of (6) is

$$\begin{aligned}\boldsymbol{C} &= (\boldsymbol{A}(\theta) \odot \boldsymbol{A}(\theta)^*)\bar{\boldsymbol{C}}_x(\boldsymbol{A}(\theta) \odot \boldsymbol{A}(\theta)^*)^{\mathrm{H}} \\ &= \bar{\boldsymbol{B}}(\theta)\bar{\boldsymbol{C}}_x\bar{\boldsymbol{B}}^{\mathrm{H}}(\theta), \end{aligned} \tag{9}$$

where $\odot$ denotes the Khatri-Rao product and defines

$$\begin{aligned}\bar{\boldsymbol{B}}(\theta) &= [\bar{\boldsymbol{b}}(\theta_1), \bar{\boldsymbol{b}}(\theta_2), \cdots, \bar{\boldsymbol{b}}(\theta_K)] \\ &= [\boldsymbol{a}(\theta_1) \otimes \boldsymbol{a}^*(\theta_1), \boldsymbol{a}(\theta_2) \otimes \boldsymbol{a}^*(\theta_2), \cdots, \boldsymbol{a}(\theta_K) \otimes \boldsymbol{a}^*(\theta_K)], \end{aligned} \tag{10}$$

where $\bar{\boldsymbol{b}}(\theta_k)$ is the extended array orientation vector.

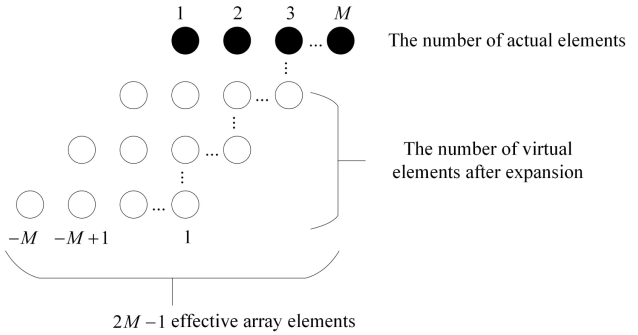

FIGURE 3. Schematic diagram of array element expansion.

B. FOURTH-ORDER CUMULATIVE DE-REDUNDANCY

There are M actual array elements in the homogeneous hydrophone array, and the fourth-order cumulative volume approach can be seen from (10), which produces a large number of virtual array elements, in which a large number of array elements overlap, and the effective number of array elements is extended to $2M-1$, and since the array aperture is extended from $(M-1)d$ to $2(M-1)d$, the discriminative power can be improved, which is conducive to the discrimination of acoustic source targets with similar orientation. The physical significance is shown in Figure 3.

Therefore, the constructed fourth-order cumulant matrix has a large number of redundant terms and high computational complexity. In this regard, a $M^2\times(2M-1)$ dimensional transformation matrix $\boldsymbol{Q}$ is constructed to remove the redundancy with the following expression:

$$\boldsymbol{Q}=[\boldsymbol{Q}_1^T,\boldsymbol{Q}_2^T,\cdots,\boldsymbol{Q}_M^T]^T, \tag{11}$$

where

$$\boldsymbol{Q}_m=\begin{cases}[\mathbf{0}_{M\times(M-1)},\mathbf{I}_M], & m=1\\ [\mathbf{0}_{M\times(M-m)},\mathbf{I}_M,\mathbf{0}_{M\times(m-1)}], & 2\le m\le M-1\\ [\mathbf{I}_M,\mathbf{0}_{M\times(M-1)}], & m=M,\end{cases} \tag{12}$$

where $\mathbf{I}_M$ is an M-dimensional unit array, then there is a correspondence $\bar{\boldsymbol{b}}(\theta_k)=\boldsymbol{Q}\boldsymbol{b}(\theta_k)$, such that the new array manifold guidance vector satisfies the conjugate symmetry structure as follows:

$$\boldsymbol{b}(\theta_k)=[e^{-j2\pi(M-1)d/\lambda\sin(\theta_k)},e^{-j2\pi(M-2)d/\lambda\sin(\theta_k)},\cdots,1,\cdots,e^{j2\pi(M-1)d/\lambda\sin(\theta_k)}]. \tag{13}$$

Define the $(2M-1)\times(2M-1)$ dimensional matrix as $\boldsymbol{G}=\boldsymbol{Q}^T\boldsymbol{Q}=diag(1,2,\cdots,M-1,M,M-1,\cdots,1)$,it can be known that $\boldsymbol{G}$ is a non-singular diagonal matrix, the use of the matrix $\boldsymbol{G}$, Q for linear transformation, we can get the de-redundant transformed fourth-order cumulant matrix $\boldsymbol{R}_4$ as

$$\begin{aligned}\boldsymbol{R}_4&=\boldsymbol{G}^{-1}\boldsymbol{Q}^T\boldsymbol{C}\boldsymbol{Q}\boldsymbol{G}^{-1}\\&=\boldsymbol{G}^{-1}\boldsymbol{Q}^T(\bar{\boldsymbol{B}}(\theta)\bar{\boldsymbol{C}}_x\bar{\boldsymbol{B}}^{\mathrm{H}}(\theta))\boldsymbol{Q}\boldsymbol{G}^{-1}\\&=\boldsymbol{G}^{-1}\boldsymbol{Q}^T(\boldsymbol{Q}\boldsymbol{B}(\theta))\bar{\boldsymbol{C}}_x(\boldsymbol{Q}\boldsymbol{B}(\theta))^{\mathrm{H}}\boldsymbol{Q}\boldsymbol{G}^{-1}\\&=\boldsymbol{B}(\theta)\bar{\boldsymbol{C}}_x\boldsymbol{B}(\theta)^{\mathrm{H}}.\end{aligned} \tag{14}$$

As a consequence, the array manifold matrix is obtained as $\boldsymbol{B}(\theta)=[\boldsymbol{b}(\theta_1),\boldsymbol{b}(\theta_2),\cdots,\boldsymbol{b}(\theta_K)]$, and the dimensions of its rows are reduced from M^2 to $2M-1$, which reduces the computational complexity to a larger extent. The matrix $\boldsymbol{R}_4$ not only utilizes all the information, but also eliminates redundant data, and the advantages of the extended array aperture are maintained. Next, to obtain an observation model with better performance, the de-redundant transformed fourth-order cumulant $\boldsymbol{R}_4$ is vectorized to obtain a single-observation vector model as follows:

$$\begin{aligned}\tilde{\boldsymbol{Z}}&=\mathrm{vec}(\boldsymbol{R}_4)=\mathrm{vec}(\boldsymbol{B}(\theta)\bar{\boldsymbol{C}}_x\boldsymbol{B}^{\mathrm{H}}(\theta))\\&=(\boldsymbol{B}^*(\theta)\odot\boldsymbol{B}(\theta))\boldsymbol{\Gamma},\end{aligned} \tag{15}$$

where $vec(\cdot)$ denotes the vectorization operator, $\boldsymbol{\Gamma}=vec(diag(\bar{\boldsymbol{C}}_x))$. If $\boldsymbol{B}^*(\theta)\odot\boldsymbol{B}(\theta)$ is used as the new array manifold matrix, the solution is still computationally intensive. There is still redundant data in this observation vector, and similarly, a $(2M-1)^2\times(4M-3)$ dimensional selection matrix $\bar{\boldsymbol{Q}}$ is constructed to downscale $\boldsymbol{\Gamma}$ twice. The construction is similar to that of $\boldsymbol{Q}$ in (11), which can be expressed as $\bar{\boldsymbol{Q}}=[\bar{\boldsymbol{Q}}_1^T,\bar{\boldsymbol{Q}}_2^T,\cdots,\bar{\boldsymbol{Q}}_{2M-1}^T]$, defining $G=\bar{Q}^T\bar{\boldsymbol{Q}}$, and similarly, we have

$$\boldsymbol{B}^*(\theta)\odot\boldsymbol{B}(\theta)=\bar{\boldsymbol{Q}}D(\theta), \tag{16}$$

where $\boldsymbol{D}(\theta)=[\boldsymbol{d}(\theta_1),\boldsymbol{d}(\theta_2),\cdots,\boldsymbol{d}(\theta_K)]$ is the new array manifold matrix after dimensionality reduction and its corresponding orientation vector is

$$\boldsymbol{d}(\theta_k)=[e^{-j2\pi(2M-2)d/\lambda\sin(\theta_k)},e^{-j2\pi(2M-3)d/\lambda\sin(\theta_k)},\cdots,1,\cdots,e^{j2\pi(2M-2)d/\lambda\sin(\theta_k)}]. \tag{17}$$

Substituting (16) into (15), the single-vector observation model is $\tilde{\boldsymbol{Z}}=\bar{\boldsymbol{Q}}D(\theta)\boldsymbol{\Gamma}$, and left-multiplying $\bar{\boldsymbol{G}}^{-1}\bar{\boldsymbol{Q}}^T$ to remove redundancy, we obtain the final vector observation model:

$$\hat{\boldsymbol{Z}}=\bar{\boldsymbol{G}}^{-1}\bar{\boldsymbol{Q}}^T\bar{\boldsymbol{Q}}D(\theta)\boldsymbol{\Gamma}=\boldsymbol{D}(\theta)\boldsymbol{\Gamma}. \tag{18}$$

Equation (18) is the new observation model after the second dimensionality reduction, $\boldsymbol{D}(\theta)$ is the new array manifold matrix, the dimension of its rows is reduced from M^2 to $4M-3$, and the effective number of array elements is extended to $4M-3$, the array aperture has been further extended, the resolving power has been further improved, and the overlapping redundant terms are removed, which reduces the computational volume and improves the model performance at the same time.

C. SPARSE REPRESENTATION SOLVING

Assuming $\tilde{\boldsymbol{\theta}}=\{\tilde{\theta}_1,\tilde{\theta}_2,\cdots,\tilde{\theta}_N\}$ is a fixed sampling grid point that can divide the spatial domain, N denotes the number of grids, and the general condition satisfies $N\gg M$, without loss of generality, such that $\tilde{\boldsymbol{\theta}}$ is uniformly distributed. Using the method of constructing $\boldsymbol{D}(\theta)$ in Section III-B to construct the overcomplete dictionary, the array manifold

matrix of the whole spatial domain can be denoted as $\tilde{\boldsymbol{D}}(\tilde{\theta}) = [\tilde{\boldsymbol{d}}(\tilde{\theta}_1), \tilde{\boldsymbol{d}}(\tilde{\theta}_2), \cdots, \tilde{\boldsymbol{d}}(\tilde{\theta}_N)]$, and then (18) can be expressed as

$$\boldsymbol{Z} = \tilde{\boldsymbol{D}}(\tilde{\theta})\tilde{\boldsymbol{\Gamma}}, \tag{19}$$

where $\tilde{\boldsymbol{\Gamma}}$ is a K-sparse vector, and the corresponding element is non-zero if and only if $\tilde{\theta}_k \in \{\theta_1, \theta_2, \cdots, \theta_K\}$. The analysis shows that if we can find $\tilde{\boldsymbol{\Gamma}}$, the DOA orientation of the target signal can be estimated by the position of the non-zero elements, so the DOA estimation problem is transformed into an l_0 paradigm optimization problem as follows:

$$\min \left\| \boldsymbol{Z} - \tilde{\boldsymbol{D}}(\tilde{\theta})\tilde{\boldsymbol{\Gamma}} \right\|_2 + \lambda \left\| \tilde{\boldsymbol{\Gamma}} \right\|_0, \tag{20}$$

where $\|\cdot\|_0$ and $\|\cdot\|_2$ denote the l_0 and l_2 paradigms, respectively, and λ denotes the regularization factor, whose value is related to the noise energy. The analysis shows that the problem is a minimum l_0 paradigm problem, solving the minimum l_0 paradigm is a Non-deterministic Polynomial problem, and the value of the solution is extremely unstable. According to the constrained isometric property, the l_0 parameter of the non-convex optimization can be replaced by the l_1 parameter and transformed into the l_1-parameter sparse constrained optimization problem as follows:

$$\min \left\| \boldsymbol{Z} - \tilde{\boldsymbol{D}}(\tilde{\theta})\tilde{\boldsymbol{\Gamma}} \right\|_2 + \lambda \left\| \tilde{\boldsymbol{\Gamma}} \right\|_1, \tag{21}$$

where $\|\cdot\|_1$ denotes the l_1 paradigm. Equation (21) is solved using the paradigm convex optimization method to obtain the sparse vector $\tilde{\boldsymbol{\Gamma}}$ and thus the orientation estimates of the K sources from the grid positions of the non-zero elements.

IV. SIMULATION AND EXPERIMENTAL ANALYSIS

A. SIMULATION TEST

The fourth-order cumulants are used in the case of Gaussian colored noise for hydroacoustic target DOA estimation using the sparse representation in this paper. The Gaussian colored noise is generated by an Auto-Regressive (AR) filter. In this paper, the colored noise is generated by using a second-order AR filter with filter coefficients of $[1, -0.2, -0.1]$. Figure 4 shows the power spectrum density function plot of the generated section of Gaussian colored noise. From the figure, it can be seen that its power spectrum is not flat and thus is colored noise. The simulation verifies that the higher-order cumulative volume can extend the array aperture, and can effectively estimate the sound source larger than the number of array elements, using the standard uniform linear hydrophone array with array element spacing of $d = \lambda/2$ and the number of array elements of $M = 5$. The six linear FM signal sources are used, i.e., $K = 6$, and the frequency bands are 90-110 Hz, 280-320 Hz, 480-520 Hz, 680-720 Hz, 880-920 Hz, 1 080-1 120 Hz, the sampling frequency is 100 kHz and the true orientation is $[-40° \ -20° \ -10° \ 5° 30° 50°]$. The number of snapshots is $T = 1000$, and the input SNR of the array element is $SNR = 10\,dB$. The spatial angle is classified as $[-\pi/2, \pi/2]$, the angular interval $r = 1°$ and the regularisation factor is 1. A comparison of the spatial spectral estimation effect obtained by the method in this paper is

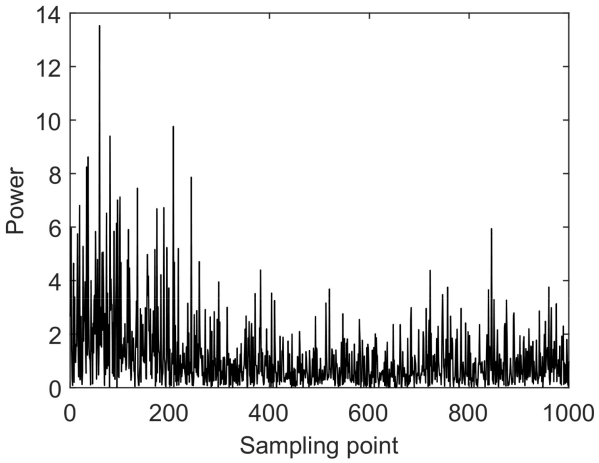

FIGURE 4. Diagram of Gaussian colored noise power spectral density.

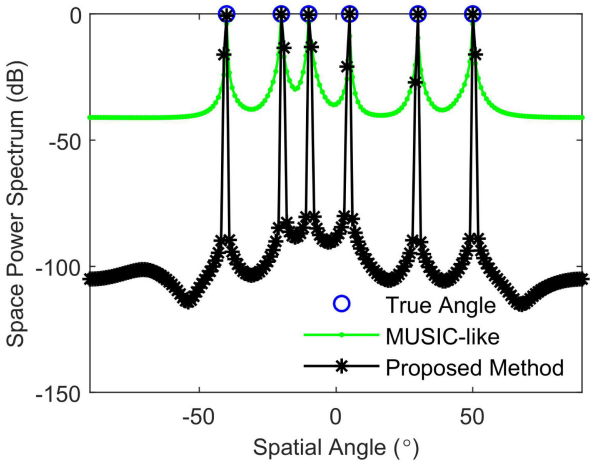

FIGURE 5. Spatial spectrum estimation after array element expansion.

shown in Figure 5. From the figure, it can be seen that in the case that the number of sources is larger than the number of array elements, both the MUSIC-like algorithm and the algorithm in this paper can estimate the orientation of the sources, which is because the fourth-order cumulative volume produces the virtual array elements, which effectively expands the aperture of the array, and therefore can effectively estimate the sources larger than the number of array elements.

Consider two linear FM sources with frequency bands of 90-110 Hz and 280-320 Hz, source incidence directions of $-10.2°$ and $25.7°$, number of snapshots of 1,000, array element input signal-to-noise ratio of $SNR = 0\,dB$, number of array elements of $M = 6$, all other conditions remain unchanged, and increase the off-grid sparse Bayesian derivation algorithm for comparison, Figure 6 shows the DOA spatial spectra of MUSIC-like algorithm under the condition of the same parameters in a single pass, OGSBI algorithm and the DOA space spectra of this paper's algorithm. As can be seen in Figure 6, the method in this paper can effectively discriminate the two-target signal angles and has a narrower

main flap width, and the estimation results of the MUSIC-like algorithm are −10°and 25°. The OGSBI algorithm can overcome the off-grid error to a certain extent, has the largest estimation error of −8.9354° and 26°, which is because the algorithm cannot effectively suppress the colored noise. And the estimation results of this paper's algorithm are −10° and 26°, obviously, this estimation result of this paper's algorithm has a smaller error and is closer to the real orientation. In Figure 6, it is evident that the proposed algorithm excels in achieving the lowest spatial power spectrum estimation. This superiority is attributed to the construction of a selection matrix and the execution of a vectorization transformation, yielding a more concise and information-rich model for the observation vector. The construction of the selection matrix enables the selective retention of crucial information, thereby enhancing the efficiency and accuracy of subsequent processing.

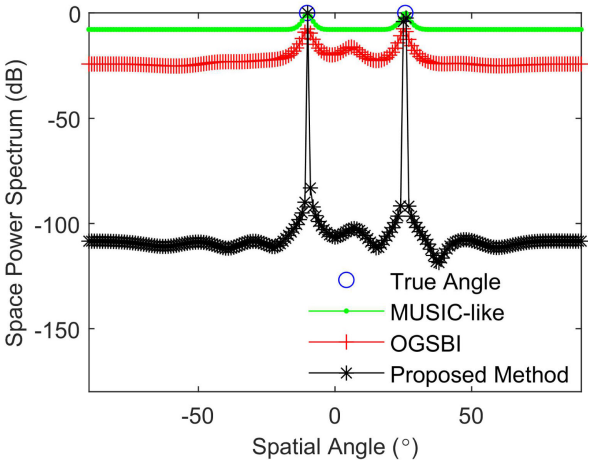

FIGURE 6. Comparison diagrams of spatial spectrum estimations by MUSIC-like, OGSBI and the proposed algorithms for the same parameters in a single pass.

Next, we compare the estimation accuracy of different methods. Defining the root-mean-square error (RMSE) as

$$\mathrm{RMSE} = \sqrt{\frac{1}{SK}\sum_{s=1}^{S}\sum_{k=1}^{K}\left(\hat{\theta}_{k_s} - \theta_k\right)^2}, \tag{22}$$

where S denotes the number of Monte Carlo experiments, K is the number of source signals, and $\hat{\theta}_{k_s}$ denotes the orientation estimate of the kth signal source in the sth experiment. Meanwhile, the Cramer–Rao lower bound (CRLB) [26] for the DOA estimation performance is also plotted as the baseline.

Figure 7 shows the variation curves of DOA estimation RMSE of the three algorithms concerning the input SNR of the array element, considering two linear FM sources with frequency bands of 90-110 Hz and 280-320 Hz, the incidence directions of −10.2° and 25.7°, and the input SNR of −3 dB, −1 dB, 1 dB, 3 dB, and 5 dB, respectively, and all other

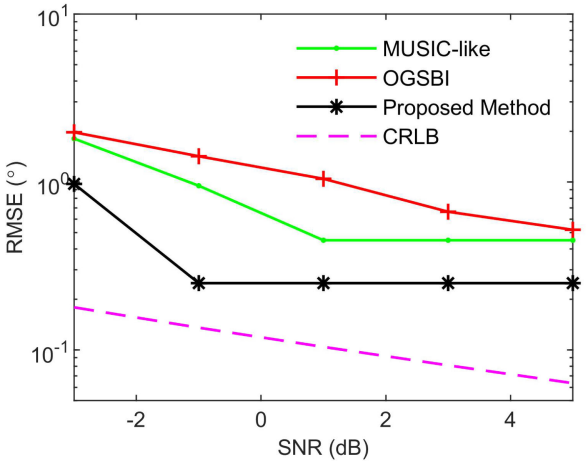

FIGURE 7. Variation curves of the root mean square error with signal-to-noise ratio for the three algorithms.

conditions remain unchanged, and the results of each simulation are obtained from 50 Monte Carlo experiments. From Figure 7, it can be learned that the DOA estimation RMSE of the OGSBI algorithm and the MUSIC-like algorithm are relatively high, which is because the OGSBI algorithm, although it can eliminate the off-grid error, targets white noise and cannot suppress the colored noise well, whereas the MUSIC-like algorithm can suppress the Gaussian colored noise to a certain extent, but the estimation accuracy is limited, especially in the low SNR conditions, the RMSE is larger. The method in this paper, on the other hand, has a lower RMSE and better suppression of colored noise. The RMSE of the three algorithms decreases as the signal-to-noise ratio of the array element input increases, which is because the interference of the noise decreases gradually, and the error at this time mainly originated from the true orientation deviation from the grid. The constancy observed in the RMSE value is attributable to the diminished sensitivity of the proposed algorithm to noise within a designated range of signal-to-noise ratios and the algorithm estimates the point with the closest bearing to the sound source each time. This characteristic underscores the algorithm's heightened robustness, thereby contributing to the augmentation of reliability in orientation estimation.

To compare the effect of the number of snapshots on the root mean square error of the DOA estimation of the three algorithms, two signal sources are used, the incidence directions are −10.2° and 25.7°, the input signal-to-noise ratio of the array element is $SNR = 0\ dB$, the number of snapshots T is set from 100 to 1 000 in steps of 100, and the simulation results are obtained from 50 Monte Carlo experiments at a time, and the changes of the RMSE of the spatial-spectral estimation results of the three algorithms with the number of snapshots are shown in Figure 8, It can be analyzed that the RMSE of the MUSIC-like and OGSBI algorithms is higher when the number of snap counts is 100, and as the number of snap counts increases, the root-mean-square error of the MUSIC-like algorithm is lower than that of the OGSBI

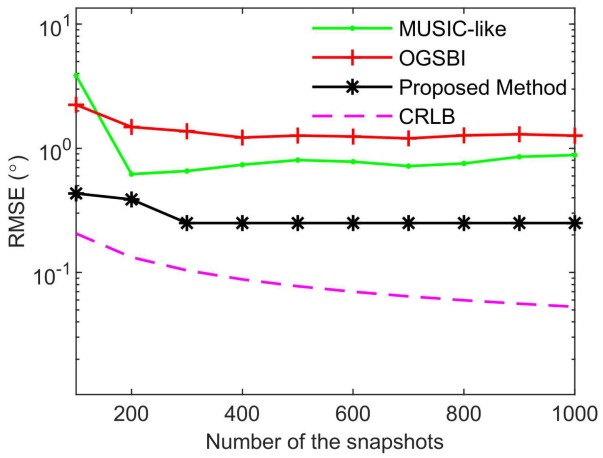

FIGURE 8. Variation curves of the root mean square error with the number of snapshots for the three algorithms.

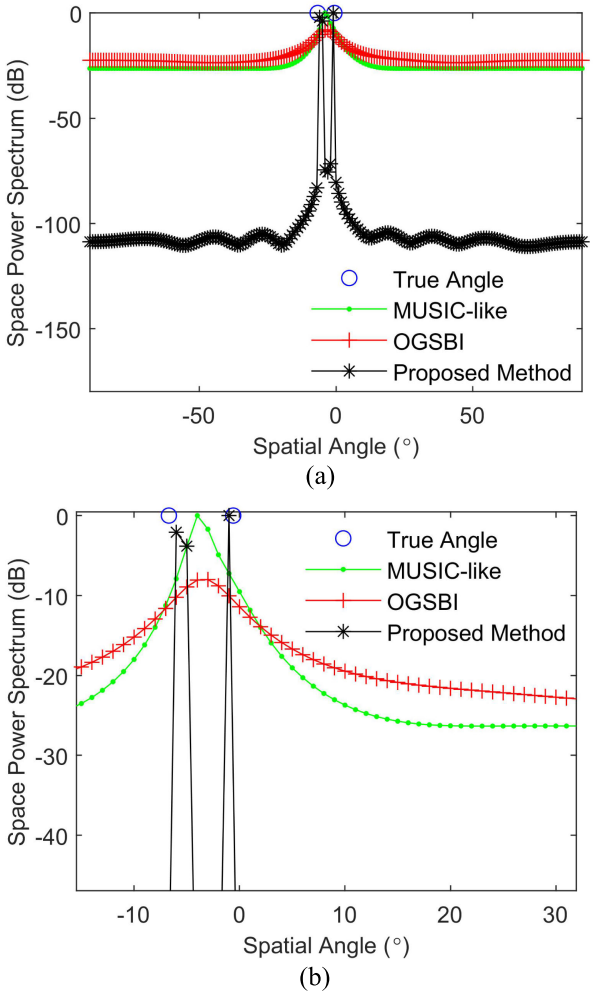

FIGURE 9. Comparison diagrams of the spatial spectral estimates of close sound sources for the three algorithms. (a) Spatial spectrum estimated of three algorithms. (b) Partial enlargement of figure (a).

algorithm, and the impact of the number of snap counts on the performance of the algorithms becomes smaller at this time, while the algorithm of the present paper, due to its use of a sparse representation model, also has a lower root-mean-square error in the condition of fewer snap counts, with a better DOA estimation performance than the other two algorithms.

Comparing the ability of this paper's algorithm to distinguish two sources with close azimuthal proximity under a uniform linear array, the number of snapshots is 1,000, the incidence directions of the two sources are $-6.7°$, $-0.6°$, the input signal-to-noise ratio of the array element is $SNR = 0dB$, the number of array elements is $M = 5$, and the single spatial-spectral estimation maps, as well as the target local zoom maps of the three algorithms, are shown in Figure 9 (a) and Figure 9 (b), respectively, and as can be seen in Figure 9, the power spectra obtained by the paper's algorithm can distinguish two sources with a similar orientation, while the power spectra corresponding to the MUSIC-like algorithm and the OGSBI algorithm cannot distinguish sources with a similar orientation, thus verifying that the method of this paper is better than the other two methods in terms of resolution.

B. EXPERIMENTAL DATA TESTING

The experimental data obtained from the sea experiment conducted in October 2014 in a sea area of the Yellow Sea of China were used for verification. On that day, there were passing ships near the experimental sea area, and there was wind-forming noise, which was analyzed and verified that the noise power spectral density fluctuated with the frequency and did not satisfy the white noise characteristics, thus was colored noise. Two buoys were used as observation points, numbered O (No.1 buoy) and M (No.2 buoy). Each buoy was equipped with three hydrophones and one transmitting acoustic source, and depth sensors were installed on each hydrophone and acoustic source to obtain their accurate seawater depths, with a depth sensor accuracy of 0.2 percent.

The water depth of the experimental sea area is 25.5 m. According to the depth sensor records, during the experiment, the sound source suspended by the O buoy is at 15 m underwater; the three hydrophones of the M buoy are arranged horizontally at 5.4 m underwater, and the spacing of the arrays is half-wavelength, and the distance of the two buoys is calculated to be 4 672 m according to the GPS data on the buoys. The transmitted signals are in the form of 4-6 kHz broadband long pulse linear FM signal with a signal length of 893 ms and a sampling frequency of 25 kHz. the true bearing is located at $-14.1°$, and the experimental deployment at sea is shown in Figure 10.

Figure 12 shows the DOA spatial spectrum estimation results of processing a section of sea trial data with a snap count of 100, the signal-to-noise ratio on the day of the experiment is about -10 dB, and the sea trial data has been pre-processed with certain noise reduction. It can be analyzed

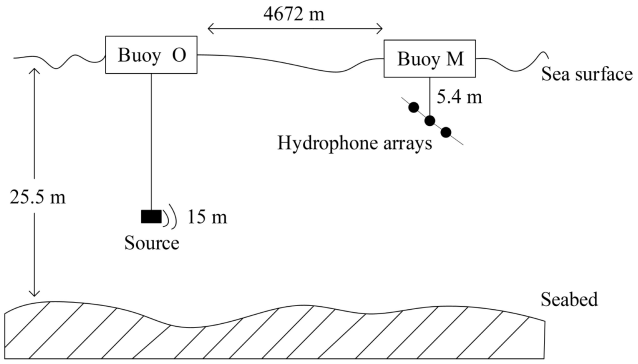

FIGURE 10. Layout of sea trial.

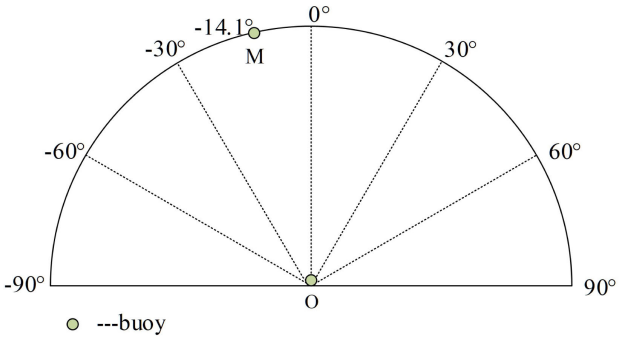

FIGURE 11. Top view of buoy azimuth.

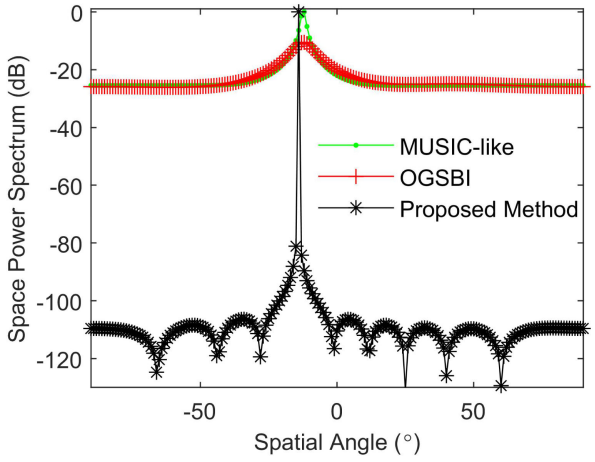

FIGURE 12. Spatial spectrums obtained from the experimental data processed by MUSIC-like algorithm, OGSBI algorithm and the proposed algorithm in this paper.

that, in the case of 100 snapshots, the bearing estimation result of MUSIC-like algorithm is $-12°$, the estimation result of OGSBI algorithm is $-12.5001°$, and the estimation result of this paper is $-14°$, and the estimation results of the three algorithms are all around $-14.1°$, which roughly matches with the actual deployment situation, and proves that this paper's algorithm can be used in the shallow sea underwater environment.

V. CONCLUSION

For the colored noise background in underwater airspace, this paper combines the fourth-order cumulant and sparse representation method for DOA estimation. In this paper, the redundant data in the fourth-order cumulant is removed by the second-fourth-order cumulant downscaling, and the sparse representation model is established for the solution, which applies to the Gaussian color noise background, and can effectively expand the array aperture. Simulation and sea trial data test show that the method in this paper is suitable for shallow sea environments, and compared with the traditional fourth-order cumulant method, the method in this paper has stronger suppression of color noise, higher resolution, and lower root-mean-square error under the condition of fewer number of snapshots and lower signal-to-noise ratio.

REFERENCES

[1] C. Xing, Y. Wu, L. Xie, and D. Zhang, "A sparse dictionary learning-based denoising method for underwater acoustic sensors," *Appl. Acoust.*, vol. 180, Sep. 2021, Art. no. 108140.

[2] X. Zhang, P. Yang, and H. Sun, "An omega-k algorithm for multireceiver synthetic aperture sonar," *Electron. Lett.*, vol. 59, no. 13, pp. 1–3, Jul. 2023.

[3] Y. Xue, H. Zhu, X. Wang, G. Zheng, X. Liu, and J. Wang, "Bayesian geoacoustic parameters inversion for multi-layer seabed in shallow sea using underwater acoustic field," *Frontiers Mar. Sci.*, vol. 10, Jan. 2023, Art. no. 1058542, doi: 10.3389/fmars.2023.1058542.

[4] X. Zhang, "An efficient method for the simulation of multireceiver SAS raw signal," *Multimedia Tools Appl.*, pp. 1–18, 2023, doi: 10.1007/s11042-023-16992-5.

[5] J. Zhu, Y. Song, N. Jiang, Z. Xie, C. Fan, and X. Huang, "Enhanced Doppler resolution and sidelobe suppression performance for Golay complementary waveforms," *Remote Sens.*, vol. 15, no. 9, p. 2452, May 2023.

[6] G. Liang, Z. Shi, L. Qiu, S. Sun, and T. Lan, "Sparse Bayesian learning based direction-of-arrival estimation under spatially colored noise using acoustic hydrophone arrays," *J. Mar. Sci. Eng.*, vol. 9, no. 2, p. 127, Jan. 2021.

[7] J. Wang and J.-G. Huang, "Adaptive matched filter detection method on underwater small aperture array," *J. Electron. Inf. Technol.*, vol. 33, no. 6, pp. 1385–1389, Jul. 2011.

[8] H. Zhu, Y. Xue, Q. Ren, X. Liu, J. Wang, Z. Cui, S. Zhang, and H. Fan, "Inversion of shallow seabed structure and geoacoustic parameters with waveguide characteristic impedance based on Bayesian approach," *Frontiers Mar. Sci.*, vol. 10, Jan. 2023, Art. no. 1104570, doi: 10.3389/fmars.2023.1104570.

[9] P. Yang, "An imaging algorithm for high-resolution imaging sonar system," *Multimedia Tools Appl.*, pp. 1–17, 2023, to be published, doi: 10.1007/s11042-023-16757-0.

[10] H. Q. Niu, Z. L. Li, and Z. X. Gong, "Sequential direction-of-arrival estimation using multi-frequency multi-snapshot sparse Bayesian learning," *Tech. Acoust.*, vol. 38, no. 5, pp. 161–162, 2019.

[11] H. L. Yang and X. Y. Gong, "Estimation method of underwater target direction-of-arrival based on compressive sensing," *Ship Electron. Eng.*, vol. 41, no. 5, pp. 44–48, 2021.

[12] X. Zhang, H. Wu, H. Sun, and W. Ying, "Multireceiver SAS imagery based on monostatic conversion," *IEEE J. Sel. Topics Appl. Earth Observ. Remote Sens.*, vol. 14, pp. 10835–10853, 2021.

[13] H. Zhu, Z. Cui, J. Liu, S. Jiang, X. Liu, and J. Wang, "A method for inverting shallow sea acoustic parameters based on the backward feedback neural network model," *J. Mar. Sci. Eng.*, vol. 11, no. 7, p. 1340, Jun. 2023.

[14] X. Xu, X. Wei, and Z. Ye, "DOA estimation based on sparse signal recovery utilizing weighted L_1-norm penalty," *IEEE Signal Process. Lett.*, vol. 19, no. 3, pp. 155–158, Mar. 2012.

[15] Z. Yang, L. Xie, and C. Zhang, "Off-grid direction of arrival estimation using sparse Bayesian inference," *IEEE Trans. Signal Process.*, vol. 61, no. 1, pp. 38–43, Jan. 2013.

[16] B. Porat and B. Friedlander, "Direction finding algorithms based on high-order statistics," *IEEE Trans. Signal Process.*, vol. 39, no. 9, pp. 2016–2024, Sep. 1991.
[17] S. J. Wu, J. Z. Zhang, and S. Zhang, "Study of array extend based on forth-order cumulant," *J. Harbin Eng. Univ.*, vol. 26, no. 3, pp. 113–116, 2005.
[18] H. Y. Song and S. C. Piao, "DOA estimation method based on orthogonal joint diagonalization of high-order cumulant," *J. Electron. Inf. Technol.*, vol. 32, no. 4, pp. 967–972, 2010.
[19] S. N. Han, D. S. Li, and A. X. Yong, "DOA estimation method by sparse representation of fourth-order cumulants," *J. Signal Process.*, vol. 31, no. 3, pp. 314–318, 2015.
[20] Q. H. Liu, X. Q. Zhou, and L. N. Jin, "The DOA estimation using non-redundant cumulants sparse representation in correlated colored noise," *Acta Aeronautica et Astronautica Sinica*, vol. 38, no. 4, pp. 212–221, 2017.
[21] H. Wang, X. Wang, L. Wan, and M. Huang, "Robust sparse Bayesian learning for off-grid DOA estimation with non-uniform noise," *IEEE Access*, vol. 6, pp. 64688–64697, 2018.
[22] M. Pan, G. Zhang, Z. Hu, and Q. Zheng, "Real-valued off-grid DOA estimation via iterative optimisation based on covariance differencing method with spatial coloured noise," *IET Radar, Sonar Navigat.*, vol. 13, no. 7, pp. 1116–1122, Jul. 2019.
[23] H. Krim and M. Viberg, "Two decades of array signal processing research: The parametric approach," *IEEE Signal Process. Mag.*, vol. 13, no. 4, pp. 67–94, Jul. 1996.
[24] S. Xie, S. X. Lin, and F. L. Huang, "Research on echo detection algorithm of underwater high-speed small targets under color noise background," *Tech. Acoust.*, vol. 33, no. 5, pp. 52–56, 1996.
[25] X. K. Li, T. T. Li, and X. Y. Gu, "Array gain of fourth-order cumulants beamforming under typical probability density background," *Acta Acustica*, vol. 39, no. 5, pp. 557–564, 2014.
[26] P. Stoica and A. Nehorai, "Performance study of conditional and unconditional direction-of-arrival estimation," *IEEE Trans. Acoust., Speech, Signal Process.*, vol. 38, no. 10, pp. 1783–1795, Oct. 1990.

CHUANXI XING was born in Heilongjiang, China, in 1982. He received the Ph.D. degree in hydroacoustic engineering from Harbin Engineering University, Harbin, China, in 2015. He is currently a Professor with Yunnan Minzu University. His research interest includes underwater acoustic signal processing.

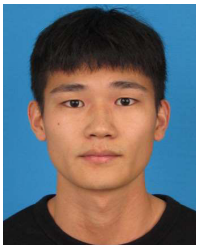

SAIMENG DONG was born in Hebei, China, in 1999. He received the B.E. degree in electronic information engineering from the Hebei University of Economics and Business, Hebei, in 2021. He is currently pursuing the master's degree in information and communication engineering with Yunnan Minzu University. His research interests include array signal processing and hydroacoustic localization.

ZHILIANG WAN was born in Jiangxi, China, in 1997. He received the B.E. degree in electronic information science and technology from Jinggangshan University, Ji'an, China, in 2019, and the M.E. degree in communication and information system from Yunnan Minzu University, in 2022. His research interests include array signal processing and hydroacoustic positioning.